We are IntechOpen,
the world's leading publisher of
Open Access books
Built by scientists, for scientists

5,000
Open access books available

125,000
International authors and editors

140M
Downloads

Our authors are among the

154
Countries delivered to

TOP 1%
most cited scientists

12.2%
Contributors from top 500 universities

BOOK CITATION INDEX

CLARIVATE ANALYTICS

INDEXED

WEB OF SCIENCE™

Selection of our books indexed in the Book Citation Index
in Web of Science™ Core Collection (BKCI)

Interested in publishing with us?
Contact book.department@intechopen.com

Numbers displayed above are based on latest data collected.
For more information visit www.intechopen.com

Chapter

High FSR and Critical Coupling Control of Microring Resonator Based on Graphene-Silicon Multimode Waveguides

Trung-Thanh Le and Duy-Tien Le

Abstract

We present a new approach for designing a compact microring resonator structure based on only one multimode waveguide, which can provide a very high free spectral range (FSR) and capability of controlling the critical coupling. The silicon on insulator (SOI) waveguide and graphene-silicon waveguide (GSW) are used for the proposed structure. By changing the applied voltage on the graphene sheet, we can achieve a full control of the critical coupling. Some important properties of the proposed microring resonator such as free spectral range and quality factor are analyzed. We show that our structure can provide all characteristics of a single microring resonator with universal applications such as optical switching, modulating, filtering and signal processing, etc.

Keywords: multimode interference (MMI), silicon on insulator, multimode waveguide, directional coupler, finite difference time difference (FDTD), finite difference method (FDM), microring resonators (MRRs), graphene

1. Introduction

In recent years, there has been intense research about ring resonators (RRs) as the building blocks for various photonic applications such as optical switches, wavelength multiplexers, routers, optical delay lines, and optical sensors [1–3]. In the literature, microring resonators with high-quality factors (Q) are required for enhanced nonlinear effects, low threshold lasing, and sensing applications. Almost all of the proposed microring resonator structures used directional couplers as coupling elements. It was shown that such devices are very sensitive to fabrication tolerance [4]. However, a very high Q is undesirable for high-speed signal processing since it can significantly limit the operational bandwidth of the system. In addition, in microring resonator structure, the coupling ratio and loss must be matched so that the ring operates near the critical coupling to achieve a high extinction ratio [5]. To obtain a high bandwidth, a solution is to use a directional coupler with a small gap between two waveguides in order to increase the coupling coefficient. However, this causes large excess mode conversion losses, limiting the flexibility of this approach [6].

Another type of coupler, namely, the 2×2 multimode interference (MMI) coupler, has been employed in ring resonators [7–10]. MMI couplers have been shown to have relaxed fabrication requirements and are less sensitive to the wavelength or polarization variations [11, 12]. In recent years, we have presented some microring resonators based on silicon waveguides using 2×2, 3×3 MMIs for the first time [4, 13–15]. It showed that the proposed devices have good performance compared with structures based on directional couplers.

In a single ring resonator, control of the critical coupling is an important requirement [16–18]. In the literature, the Mach-Zehnder (MZI) configuration is used for this purpose [17]. The key physical mechanism they rely on is the plasma dispersion effect or thermo-optic effect. Another approaches used to create phase shifter are based on silicon-organic hybrid slot waveguides [19] and BTO-Si slot waveguides [20]. The major drawbacks of these schemes are relatively large dimensions. In addition, plasma dispersion can only induce a small variation of the refractive index; the long length of the phase shifter is required. In this chapter, we use the graphene-silicon waveguide (GSW) for phase shifter and controlling the coupling coefficient.

It is noted that in the literature, the MZI configuration for critical coupling control is based on two 3 dB 2×2 directional couplers or 2×2 MMI coupler. In this chapter, we do not need to use the MZI for controlling the critical coupling of microring resonators, but we present a new way of achieving the critical coupling based on architecture itself. Our approach has advantages of compact size and ease of fabrication with the current CMOS circuit.

In addition, we use the graphene-silicon waveguide for the phase control. Graphene is a single-sheet carbon atom in a hexagonal lattice [21]. Graphene has some potential properties for optical devices. Graphene is a 2-D single-layer carbon atoms arranged in a hexagonal lattice that has raised considerable interest in recent years due to its remarkable optical and electronic properties. For example, graphene has a much higher electron mobility than silicon [22–24]. In particular, it has a linear dispersion relationship in the so-called Dirac points where electrons behave as fermions with zero mass. As a result, we can design optical switches or modulators based on this property. Graphene can also absorb light over a broad-frequency range, so this enables high-speed applications. The density of states of carriers near the Dirac point is low, and the Fermi energy can be tuned significantly with relatively low applied voltage. The Fermi-level tuning changes the refractive index of the graphene. Therefore, the graphene sheet integrated with optical waveguide such as silicon on insulator (SOI) waveguide can provide the possibilities of programmable in optoelectronics.

2. Microring resonator based on multimode waveguides

2.1 Device structure

A new optical microring resonator based on only one multimode waveguide with four ports is shown in **Figure 1**.

Figure 2(a) shows the single-mode waveguide profile. We use silicon on insulator waveguide with a width of 500 nm and height of 250 nm for input and output waveguides. For a multimode waveguide, we use a wider width of $W_{MMI} = 6\mu m$. The field profile of the fundamental mode of the SOI waveguide is shown in **Figure 2(b)**. The refractive indices of silicon and silicon oxide used in our simulations are $n_{Si} = 3.45$, $n_{SiO2} = 1.45$. The field profiles of the fundamental mode and the first-order mode of the multimode waveguide are shown in **Figure 2(c)** and **(d)**.
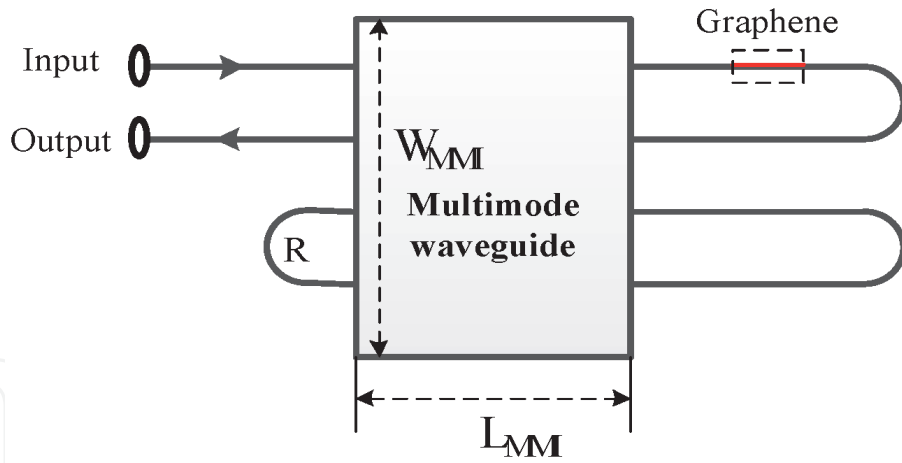
Figure 1.
Microring resonator based on only one multimode waveguide structure.
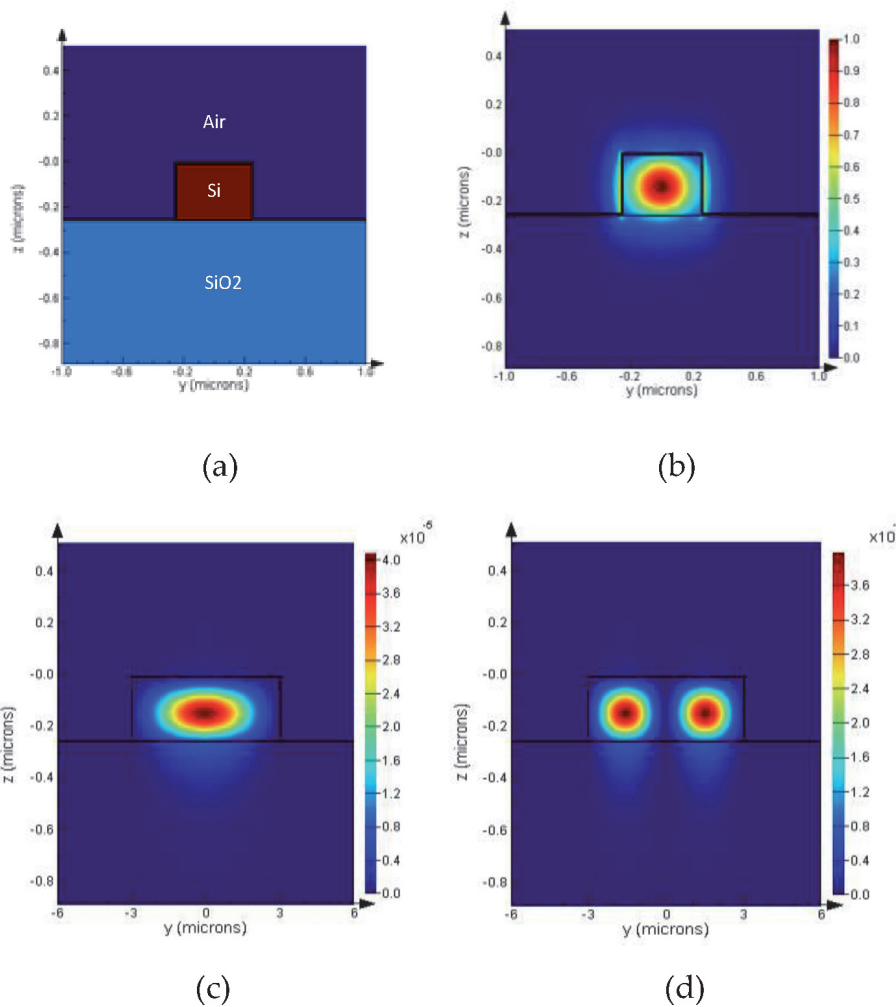

(a)

(b)

(c)

(d)

Figure 2.
(a) SOI waveguide structure, (b) field profile of the single-mode SOI waveguide, (c) fundamental mode of the multimode waveguide, and (d) the first-order mode of the multimode waveguide.

In this structure, we use a bent waveguide to connect input port 3 to port 4 as a ring resonator waveguide. Because port 3 is very near to port 4, the bent waveguide radius is relatively small. Therefore, our structure can provide a very high free spectral range (FSR), which is suitable for high-speed communications.

In the next section, we show that our structure can act like a microring resonator. In order to control the critical coupling, we use graphene integrated with silicon

waveguide. Graphene can be incorporated into silicon to implement graphene-silicon waveguide. The length of the graphene waveguide is L_{arm}. The cross-section view of the graphene-silicon waveguide is shown in **Figure 3(a)**. The GSW has a monolayer graphene sheet of 340 nm on top of a silicon waveguide, separated from it by a thin Al_2O_3 layer. Graphene, Al_2O_3, and silicon together formed a capacitor structure, which was the basic block of the graphene modulator and phase shifter [25]. The refractive index of Al_2O_3 used in our simulations is 1.6 at the operating wavelength of 1550 nm.

For example, the field profile of the waveguide with a chemical potential $\mu_c = 0.45eV$ is shown in **Figure 3(b)**.

In a multimode waveguide, the information of the image position in the x direction and phases of the output images is very important. We need to know where the multi-images appear in order to design output waveguides to capture the optical output. Furthermore, phase information of the spot images or output images is important for such devices as MMI switch. It can be shown that the field in the multimode region will be of the form [12]

$$f(x, L_{MMI}) = \frac{1}{\sqrt{N}} \sum_{p=0}^{N-1} f_{in}(x - x_p) \exp\left(-j\varphi_p\right) \tag{1}$$

where $x_p = b(2p - N)\frac{W_{MMI}}{N}, \varphi_p = b(N - p)\frac{p\pi}{N}; f_{in}(x)$ describes the field profile at the input of the multimode region; x_p and φ_p describe the positions and phases, respectively, of N self-images at that output of the multimode waveguide; p denotes the output image number; and b describes a multiple of the imaging length. For short device, we choose b = 1.

Consider a 4×4 multimode waveguide with the length of $L = L_{MMI} = \frac{3L_\pi}{2}$, where $L_\pi = \frac{\pi}{\beta_0 - \beta_1}$ is the beat length of the MMI and β_0, β_1 are the propagation constants of the fundamental and first-order modes supported by the multimode waveguide with a width of W_{MMI}. The phases associated with the images from input i to output j can be presented by

$$\varphi_{ij} = -\frac{\pi}{2}(-1)^{i+j+4} + \frac{\pi}{16}\left[i + j - i^2 - j^2 + (-1)^{i+j+4}\left(2ij - i - j + \frac{1}{2}\right)\right] \tag{2}$$
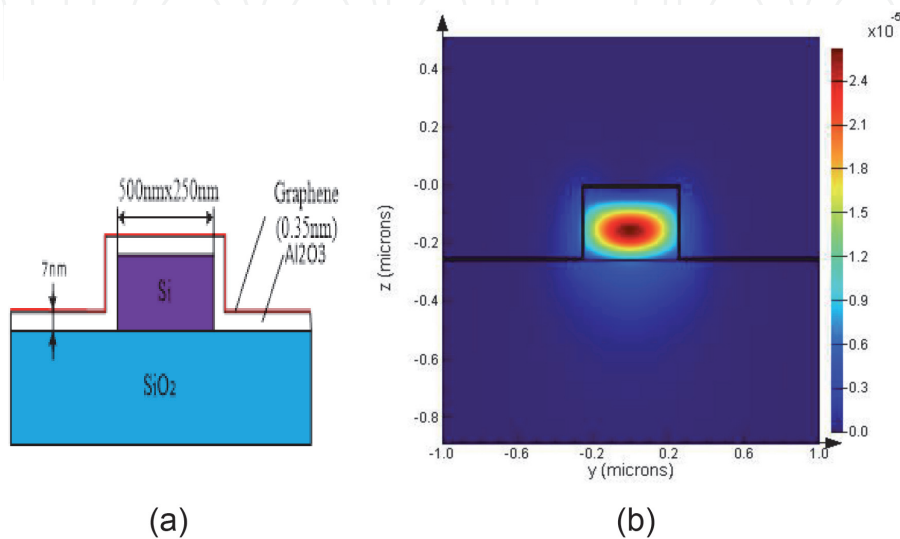

(a)   (b)

Figure 3.
(a) Graphene-silicon waveguide structure and (b) field profile with a chemical potential of $\mu_c = 0.45eV$.

We showed that the characteristics of an MMI device can be described by a transfer matrix [2]. This transfer matrix is a very useful tool for analyzing cascaded MMI structures. Phase ϕ_{ij} is associated with imaging an input i to an output j in an MMI coupler. These phases ϕ_{ij} form a matrix S_{4x4}, with i representing the row number and j representing the column number. A single 4×4 MMI coupler at a length of $L_{MMI} = \frac{3L_\pi}{2}$ is described by the following transfer matrix [26, 27]:

$$S_{4x4} = \frac{1}{2} \begin{bmatrix} 1-j & 0 & 0 & 1+j \\ 0 & 1-j & 1+j & 0 \\ 0 & 1+j & 1-j & 0 \\ 1+j & 0 & 0 & 1-j \end{bmatrix} \tag{3}$$

The output and input amplitudes at four ports of the 4×4 multimode waveguide can be expressed by

$$\overrightarrow{E_{out}} = \begin{pmatrix} E_{out,1} \\ E_{out,2} \\ E_{out,3} \\ E_{out,4} \end{pmatrix} = \mathbf{S}_{4x4} \begin{pmatrix} E_{in,1} \\ E_{in,2} \\ E_{in,3} \\ E_{in,4} \end{pmatrix} = \mathbf{S}_{4x4}\overrightarrow{E_{in}} \tag{4}$$

where $E_{in,i}$ (i = 1, 2, 3, 4) and $E_{out,j}$ (j = 1, 2, 3, 4) are complex amplitudes at input ports and output ports 1–4, respectively. From Eqs. (3) and (4), we can calculate the relations ships between the input and output amplitudes of **Figure 1** as follow:

$$\begin{pmatrix} E_{in,1} \\ E_{in,4} \end{pmatrix} = \mathbf{M} \begin{pmatrix} E_{in,2} \\ E_{in,3} \end{pmatrix} = e^{j\frac{\Delta\varphi}{2}} \begin{bmatrix} \tau & \kappa \\ \kappa^* & -\tau^* \end{bmatrix} \begin{pmatrix} E_{in,2} \\ E_{in,3} \end{pmatrix} \tag{5}$$

where $\tau = \cos\left(\frac{\Delta\varphi}{2}\right)$, and $\kappa = \sin\left(\frac{\Delta\varphi}{2}\right)$, $\Delta\varphi$ is the phase difference between the graphene-silicon waveguide with the length of L_{arm} and the silicon on insulator waveguide and can be calculated by [28]

$$\Delta\varphi = \frac{2\pi}{\lambda} \Delta n_{eff} L_{arm} \tag{6}$$

The phase difference $\Delta\varphi$ can be controlled by applying a voltage V_g to the graphene sheet. The field propagation of the multimode waveguide for input ports 1 and 2 is shown in **Figure 4**. The optimal length of the MMI is calculated by the 3D-BPM [29]. We show that the optimal length is found to be 214 μm.
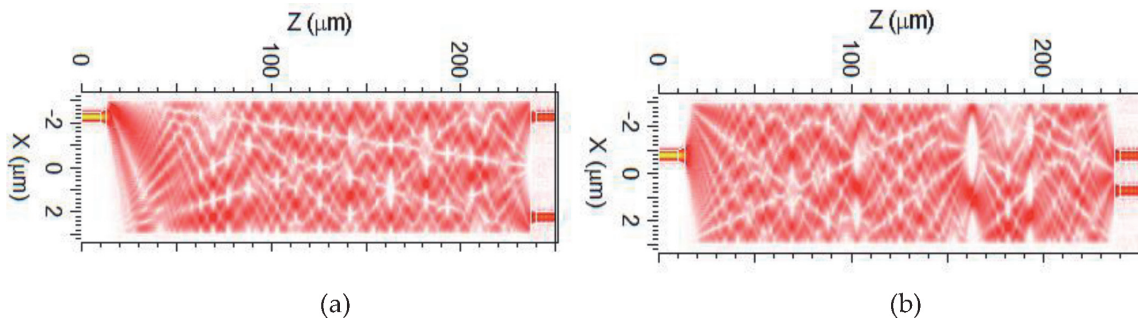

Figure 4.
Field propagation of 4 × 4 MMI coupler: (a) field propagation, in 1, and (b) field propagation, in 2.
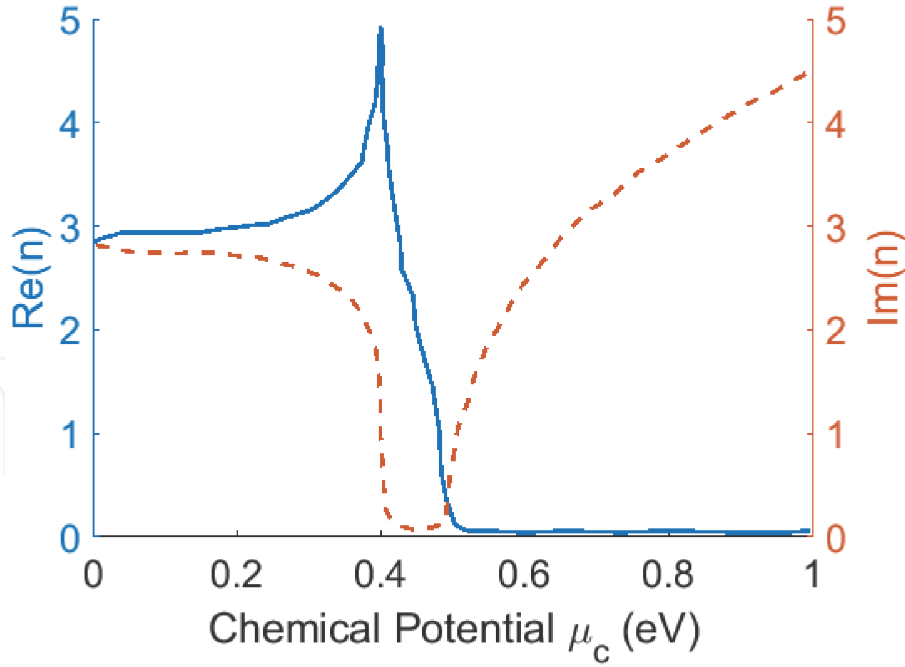
Figure 5.
Refractive index of graphene sheet.

The light propagation through the resonator is characterized by a round-trip transmission $E_{in,3} = \alpha \exp{(j\theta)}E_{in,4}$, where $\theta = \frac{2\pi}{\lambda} n_{eff} L_R$ is the round-trip phase, α is the loss factor, n_{eff} is the effective refractive index of the SOI single-mode waveguide, and L_R is the ring resonator circumference. The normalized transmitted power of the device can be calculated by

$$T = \left|\frac{E_{in,2}}{E_{in,1}}\right|^2 = \frac{\alpha^2 - \cos^2(\Delta\varphi/2) - 2\alpha|\cos{(\Delta\varphi/2)}|\cos{(\theta)}}{1 + \alpha^2 \cos^2(\Delta\varphi/2) - 2\alpha|\cos{(\Delta\varphi/2)}|\cos{(\theta)}} \tag{7}$$

At resonance wavelengths when $\theta = 2m\pi$, m $= 1, 2, 3, \ldots$, the normalized power transmission is

$$T = \left|\frac{E_{in,2}}{E_{in,1}}\right|^2 = \frac{|\alpha - |\cos{(\Delta\varphi/2)}||^2}{|1 - \alpha|\cos{(\Delta\varphi/2)}||^2} \tag{8}$$

2.2 Graphene-silicon waveguide

The presence of the graphene layer changes the propagation characteristics of the guided modes, and these can be controlled and reconfigured, changing the chemical potential by means of applying a suitable voltage V_g. The real and image parts of the refractive index of graphene with different chemical potentials are shown in **Figure 5** [30].

Graphene has optical properties due to its band structure that provides both intraband and interband transitions. Both types of the transitions contribute to the material conductivity expressed by

$$\sigma(\omega) = \sigma_{\text{intra}}(\omega) + \sigma_{\text{inter}}(\omega) \tag{9}$$

where $\sigma_{\text{intra}}(\omega)$ and $\sigma_{\text{inter}}(\omega)$ are the intraband and interband conductivities, which can be calculated by the Kubo's theory:

$$\sigma_{\text{intra}}(\omega) = \frac{ie^2}{\pi\hbar(\omega + i2\Gamma)}\left[\frac{\mu_c}{k_BT} + 2\ln\left(e^{-(\mu_c/k_BT)} + 1\right)\right] \qquad (10)$$

$$\sigma_{\text{inter}}(\omega) = -\frac{ie^2}{4\pi\hbar}\ln\left(\frac{2|\mu_c| - (\omega - 2i\Gamma)\hbar}{2|\mu_c| + (\omega - 2i\Gamma)\hbar}\right) \qquad (11)$$

where e is electron charge, $\hbar$ is the angular Planck constant, k_B is the Boltzmann constant, T is the temperature, μ_c is the Fermi level or chemical potential, $\Gamma = \frac{eV_F^2}{\mu\mu_c}$ is the electron collision rate, μ is electron mobility, and V_F is the Fermi velocity in graphene.

The dielectric constant of a graphene layer can be calculated by [21, 22]

$$\varepsilon_g(\omega) = 1 + \frac{i\sigma(\omega)}{\omega\varepsilon_0\Delta} \qquad (12)$$

The refractive index of the graphene layer sheet can be changed by providing the applied voltage V_g to the graphene sheet. It is because it will change the value of the chemical potential:

$$\left|\mu_c(V_g)\right| = \hbar V_F\sqrt{\pi|\eta(V_g - V_0)|} \qquad (13)$$

where V_0 is the offset voltage from zero caused by natural doping.

2.3 Critical coupling control

It is shown that the normalized transmission T through the device can be switched from unity to zero at the condition of critical coupling, given by $\alpha = |\tau|$. The control of the phase shift $\Delta\varphi$, so the condition of the critical coupling is met, can be achieved through applying voltage to the graphene sheet. The effective index of the graphene-silicon waveguide calculated at different chemical potentials by FDM method is shown in **Figure 6**. We see that for low-loss waveguide, the
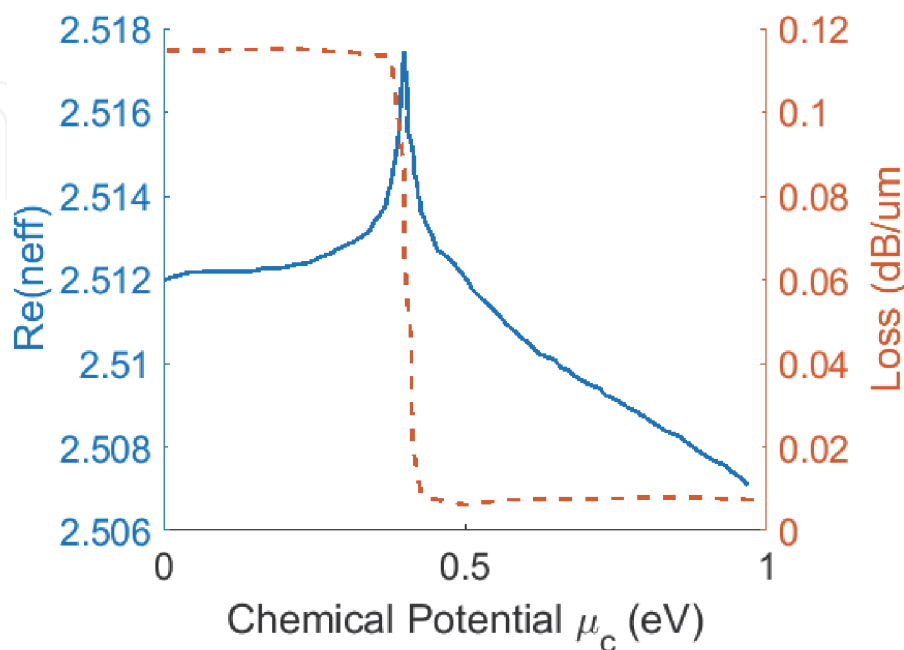

Figure 6.
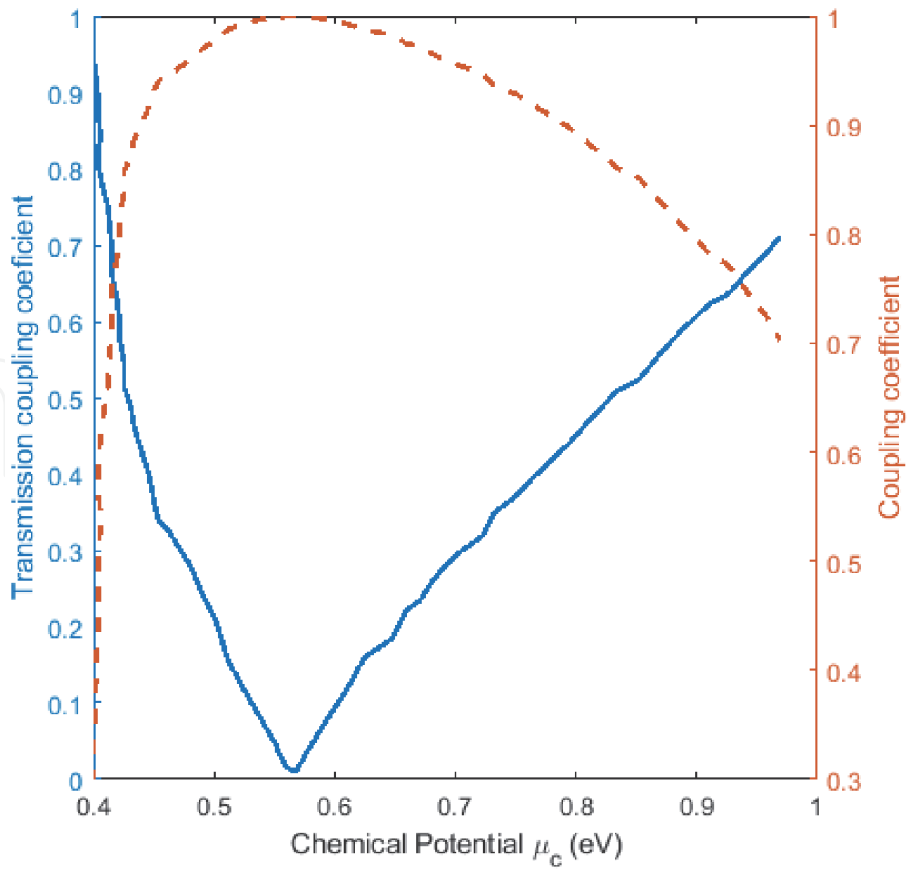*Effective refractive index of the GSW waveguide.*

Figure 7.
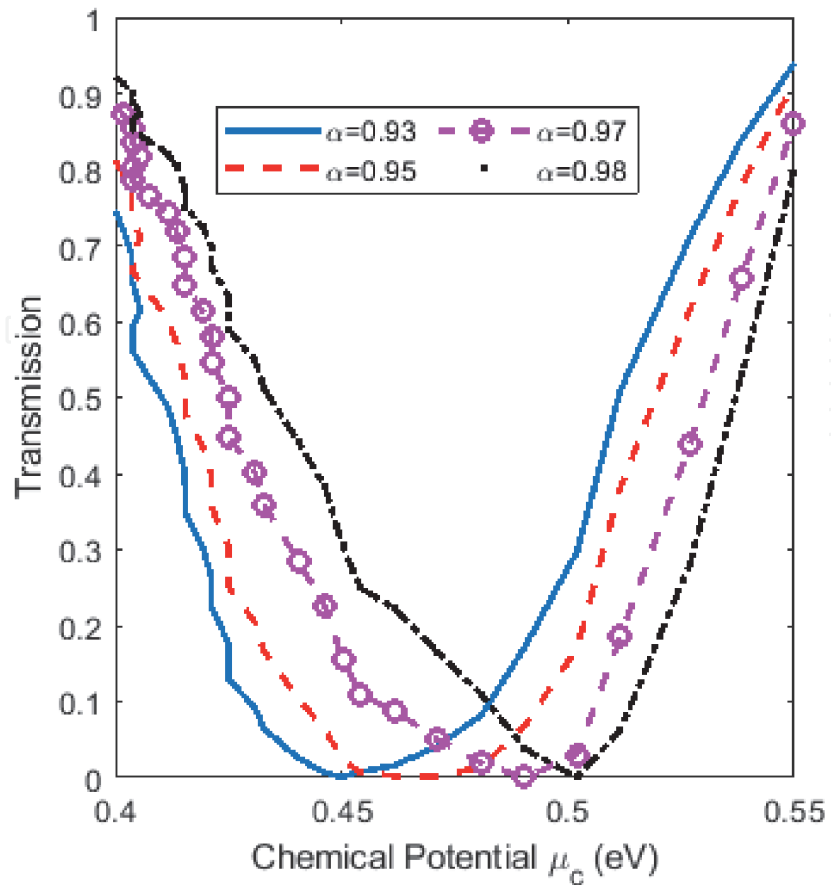*Transmission and coupling coefficients of the resonator with different chemical potentials.*

Figure 8.
Transmissions of the microring resonator with different chemical potential and loss factor.

8

chemical potential should be larger than $\mu_c = 0.4 eV$. By changing the chemical potential, the transmission and coupling coefficients $|\tau|$, $|\kappa|$ can be changed as shown in **Figure 7**. The simulations show that we can get full control of the coupling coefficient from zero to unity by changing the chemical potential from $\mu_c = 0.4 eV$ to $\mu_c = 0.58 eV$.

The transmissions of the device at different chemical potentials and loss factors are shown in **Figure 8**. The simulations have two very important features which are the key for most of the proposed applications: (1) The transmitted power is zero at a value of critical coupling, and (2) for high-quality factor, the portion of the curve to the right of the critical coupling point is steep. Small changes of the phase shifter can control the transmitted power and switch between unity and zero [17]. This chapter shows that we can achieve high-speed devices based on our proposed microring resonator.

Some other performance parameters of the microring resonator are finesse, Q-factor, resonance width, and bandwidth. These are all terms that are mainly related to the full width at half of the maximum (FWHM) of the transmission. The quality factor Q of the microring resonator of the structure in **Figure 1** can be derived as [3]

$$Q = \frac{\pi N_g L_R}{\lambda} \frac{\sqrt{\alpha\tau}}{1 - \alpha\tau} \qquad (14)$$

Another important parameter for microring resonators is the finesse F, which is defined and calculated for the single- and add-drop microring resonators by

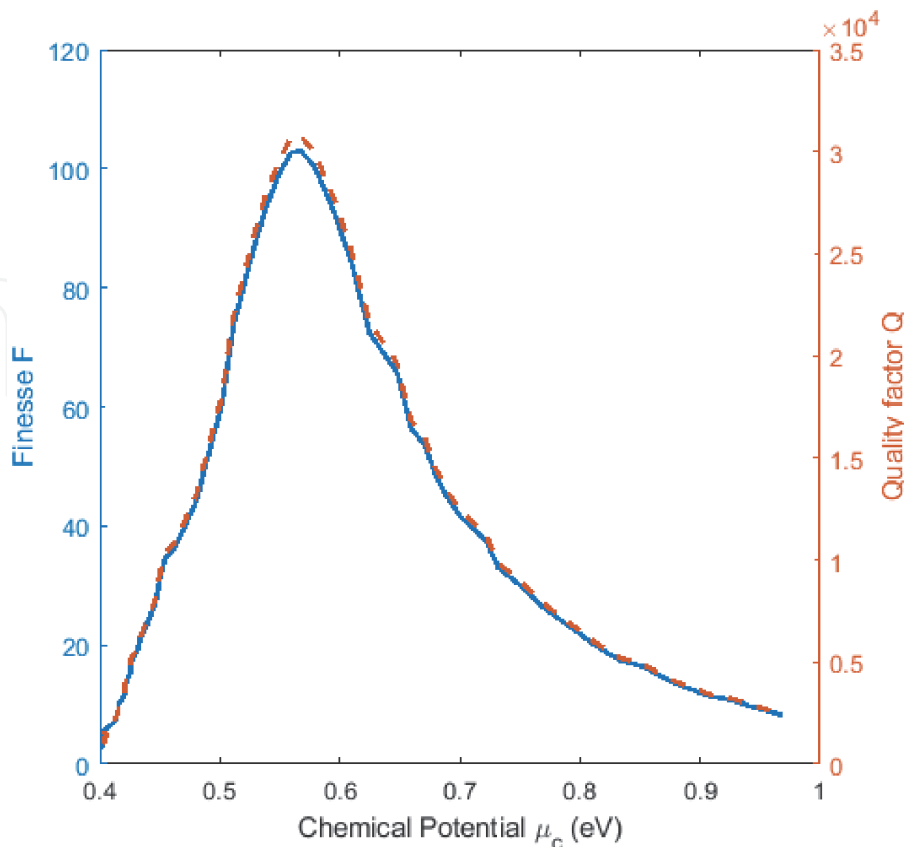$$F = \frac{FSR}{\Delta\lambda_{FWHM}} = \pi \frac{\sqrt{\alpha\tau}}{1 - \alpha\tau} \qquad (15)$$

Figure 9.
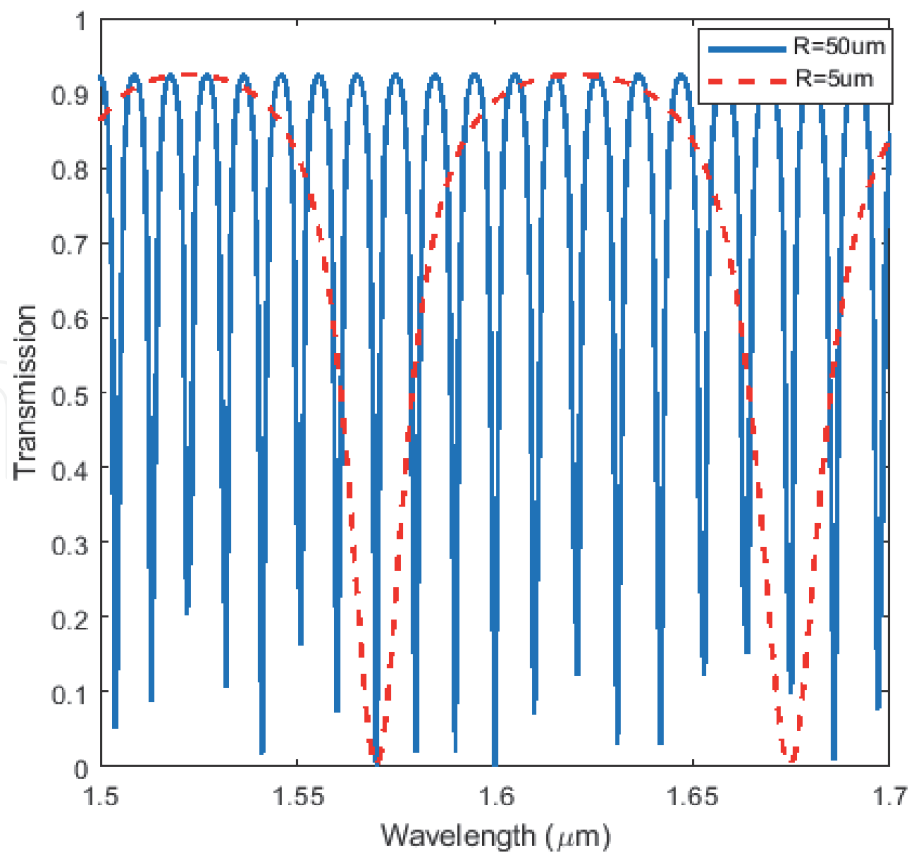*Finesse and quality factor at different chemical potentials.*

Figure 10.
Transmissions of the microring resonator with two microring radii of 5μm and 50μm.

where $\Delta\lambda_{FWHM}$ is the resonance full width at half maximum and FSR is the free spectral range. The free spectral range is the distance between two peaks on a wavelength scale. By differentiating the equation $\varphi = \beta L_R$, we get $FSR = \frac{\lambda^2}{n_g L}$, where the group index $n_g = n_{eff} - \lambda\frac{dn_{eff}}{d\lambda}$.

Figure 9 shows the finesse and quality factor with different chemical potential at a radius of $5\mu m$. We see that a maximum finesse and quality factor can be achieved at a chemical potential of $\mu_c = 0.57eV$.

The normalized transmissions of the propose microring resonator in **Figure 1** at microring radii of $5\mu m$ and $50\mu m$ are shown in **Figure 10**. Here we assume that the chemical potential is $\mu_c = 0.45eV$. The simulations show that the exact characteristics of a single microring resonator can be achieved.

Finally, we use FDTD method to simulate the proposed microring resonator based on multimode waveguide. In our FDTD simulations, we take into account the wavelength dispersion of the silicon waveguide. A light pulse of 15 fs pulse width is launched from the input to investigate the transmission characteristics of the device. The grid sizes Δx = Δy = Δz = 20 nm are chosen in our simulations for
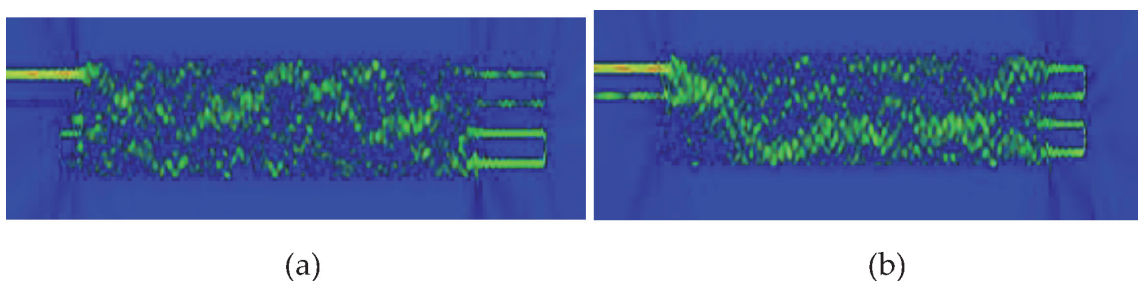

(a)   (b)

Figure 11.
Optical field propagation through the coupler for input signal presented at (a) port 1 and (b) port 2.

accurate simulations [31]. The FDTD simulations for the proposed microring resonator with chemical potential of 0.45 and 0.42 eV are shown in **Figure 11(a)** and **(b)**. The simulations show that the device operation has a good agreement with our prediction by analytical theory.

3. Conclusions

We presented a new microring resonator based on only one multimode waveguide. The critical control of the microring resonator can be achieved by using graphene-silicon waveguide. The proposed device has all characteristics of a traditional microring resonator. Some important parameters of the proposed device such as finesse, quality factor, etc. are also presented in this chapter. The device operation has been verified by using the FDTD. This microring resonator structure is very compact and can be useful for further applications in optical switching, filtering, and sensing.

Acknowledgement

Author details

Trung-Thanh Le* and Duy-Tien Le
International School (VNU-IS), Vietnam National University (VNU), Hanoi, Vietnam

*Address all correspondence to: thanh.le@vnu.edu.vn

IntechOpen

References

[1] Le T-T. Two-channel highly sensitive sensors based on 4 × 4 multimode interference couplers. Photonic Sensors. 2017;**20**:1-8. DOI: 10.1007/s13320-017-0441-1

[2] Le T-T. Multimode Interference Structures for Photonic Signal Processing. Denmark: LAP Lambert Academic Publishing; 2010

[3] Chremmos I, Schwelb O, Uzunoglu N, editors. Photonic Microresonator Research and Applications. New York: Springer; 2010

[4] Le D-T, Le T-T. Fano resonance and EIT-like effect based on 4x4 multimode interference structures. International Journal of Applied Engineering Research. 2017;**12**(13):3784-3788

[5] Yariv A. Universal relations for coupling of optical power between microresonators and dielectric waveguides. Electronics Letters. 2000;**36**:321-322

[6] Vlasov Y, McNab S. Losses in single-mode silicon-on-insulator strip waveguides and bends. Optics Express. 2004;**12**:1622-1631

[7] Xu DX, Densmore A, Waldron P, Lapointe J, Post E, Delâge A. High bandwidth SOI photonic wire ring resonators using MMI coupler. Optics Express. 2007;**15**:3149-3155

[8] Cahill L, Le T. The design of signal processing devices employing SOI MMI couplers. In: Proceedings of the SPIE of Paper 7220–2, Integrated Optoelectronic Devices (OPTO 2009), Photonics West. San Jose, California, USA: San Jose Convention Center; 2009. pp. 24-29

[9] Cahill LW, Le TT. MMI devices for photonic signal processing. In: 9th International Conference on Transparent Optical Networks (ICTON 2007). Rome, Italy; 2007. pp. 202-205

[10] Le TT, Cahill LW. Microresonators based on 3x3 restricted interference MMI couplers on an SOI platform. In: The IEEE LEOS Conference, 2009 (LEOS '09), Belek-Antalya. Turkey; 2009. pp. 479-480

[11] Soldano LB. Multimode interference couplers [PhD Thesis]. Delft, the Netherlands: Delft University of Technology; 1994

[12] Bachmann M, Besse PA, Melchior H. General self-imaging properties in N x N multimode interference couplers including phase relations. Applied Optics. 1994;**33**(18):3905-3911

[13] Le T-T. Microring resonator based on 3x3 general multimode interference structures using silicon waveguides for highly sensitive sensing and optical communication applications. International Journal of Applied Sciences and Engineering. 2013;**11**: 31-39

[14] Le T-T, Cahill L. Generation of two Fano resonances using 4x4 multimode interference structures on silicon waveguides. Optics Communications. 2013;**301-302**:100-105

[15] Le D-T, Do T-D, Nguyen V-K, Nguyen A-T, Le T-T. Sharp asymmetric resonance based on 4x4 multimode interference coupler. International Journal of Applied Engineering Research. 2017;**12**(10):2239-2242

[16] Choi JM, Lee RK, Yariv A. Control of critical coupling in a ring resonator–fiber configuration: Application to wavelength-selective switching, modulation, amplification, and oscillation. Optics Letters. 2001;**26**: 1236-1238

[17] Yariv A. Critical coupling and its control in optical waveguide-ring resonator systems. IEEE Photonics Technology Letters. 2002;**14**:483-485

[18] Le T-T. Control of critical coupling in 3x3 mmi couplers based on optical microring resonators and applications to selective wavelength switching, modulation, amplification and oscillation. Journal of Science and Technology. 2017;**6**:24-28

[19] Steglich P, Mai C, Villringer C, Pulwer S, Casalboni M, Schrader S, et al. Quadratic electro-optic effect in silicon-organic hybrid slot-waveguides. Optics Letters. 2018;**43**:3598-3601

[20] Abel S, Eltes F, Ortmann JE, Messner A, Castera P, Wagner T, et al. Large Pockels effect in micro- and nanostructured barium titanate integrated on silicon. Nature Materials. 2019;**18**:42-47

[21] Hanson GW. Dyadic Green's functions and guided surface waves for a surface conductivity model of graphene. Journal of Applied Physics. 2008;**103**:064302

[22] Capmany J, Domenech D, Muñoz P. Silicon graphene Bragg gratings. Optics Express. 2014;**22**:5283-5290

[23] Midrio M, Galli P, Romagnoli M, Kimerling LC, Michel J. Graphene-based optical phase modulation of waveguide transverse electric modes. Photonics Research. 2014;**2**:A34-A40

[24] Xing P, Ooi KJA, Tan DTH. Ultra-broadband and compact graphene-on-silicon integrated waveguide mode filters. Scientific Reports. 2018;**8**:9874

[25] Bao Q. 2D Materials for Photonic and Optoelectronic Applications. United Kingdom: Woodhead Publishing; 2019

[26] Le T-T. Two-channel highly sensitive sensors based on 4×4 multimode interference couplers. Photonic Sensors. 2017;**7**:357-364

[27] Le T-T, Cahill L. The design of 4×4 multimode interference coupler based microring resonators on an SOI platform. Journal of Telecommunications and Information Technology. 2009;**2**:98-102

[28] Petrone G, Cammarata G. Modelling and Simulation. UK: InTech Publisher; 2008

[29] Le T-T. An improved effective index method for planar multimode waveguide design on an silicon-on-insulator (SOI) platform. Optica Applicata. 2013;**43**:271-277

[30] Amin R, Ma Z, Maiti R, Khan S, Khurgin JB, Dalir H, et al. Attojoule-efficient graphene optical modulators. Applied Optics. 2018;**57**:D130-D140

[31] Rumley S, Bahadori M, Polster R, Hammond SD, Calhoun DM, Wen K, et al. Optical interconnects for extreme scale computing systems. Parallel Computing. 2017;**64**:65-80